A Method for Measuring Gravitational Potential of Satellite's Orbit Using Frequency Signal Transfer Technique between Satellites

Ziyu Shen [1], Wenbin Shen [2,*], Xinyu Xu [2], Shuangxi Zhang [2], Tengxu Zhang [1], Lin He [1], Zhan Cai [1], Si Xiong [1] and Lingxuan Wang [1]

[1] School of Resource, Environmental Science and Engineering, Hubei University of Science and Technology, Xianning 437100, China; zyshen@hbust.edu.cn (Z.S.)

[2] Time and Frequency Geodesy Center, Department of Geophysics, School of Geodesy and Geomatics, Wuhan University, Wuhan 430079, China; xyxu@sgg.whu.edu.cn (X.X.)

[*] Correspondence: wbshen@sgg.whu.edu.cn

Abstract: We introduce an approach for the direct measurement of the gravitational potential (GP) along the trajectory of a satellite, with a specific focus on Low-Earth Orbit (LEO) satellites. A LEO satellite communicates with several Geosynchronous Equatorial Orbit (GEO) satellites via frequency signal links. The GP difference can be measured in real-time using the gravitational frequency shift approach by equipping both LEO and GEO satellites with precise atomic clocks. Since the GP at the high orbits of the GEO satellites can be precisely determined by the present gravitational field model EGM2008, the GP along the LEO satellite's trajectory can be determined. In this study, simulation experiments were conducted, featuring a GRACE-type satellite as the LEO satellite in communication with three equidistant GEO satellites. The results indicated that the accuracy of the GP measurements along the LEO satellite's trajectory primarily depends on the precision of the onboard atomic clocks. Supposing optical atomic clocks attain an instability level of $1 \times 10^{-17}\tau^{-1/2}$ (τ in seconds), we determined the GP distribution covered by the LEO satellite's trajectories with 30-day observations. Then, we determined a gravitational field at the centimeter level based on the GP distribution. The GP data derived from the trajectory of a LEO satellite can be utilized to establish temporal gravitational fields, which have broad applications in different disciplines.

Keywords: relativity; satellite; gravitational potential; frequency link

1. Introduction

The Earth's gravitational field, a fundamental physical field, plays a vital role in numerous applications across various fields, rendering its determination imperative within the geodetic community. The gravitational potential (GP) field, a consequence of the Earth's density distribution, can be determined inside and outside the Earth, essentially across the entire spatial domain, by applying the Newtonian integral formula. As a result, the gravitational field throughout the space is established by applying the gradient operator to the GP field. However, the Earth's density distribution, as per the preliminary reference Earth model (PREM) [1], has been inadequately determined, making the gravitational field based on this distribution insufficient for general application requirements. Fortunately, the Earth's external gravitational field can be established by considering certain gravitation-related distributions, such as gravitation or potential distributions, over the Earth's surface (boundary) [2]. Determining a gravitational field (or GP field) based on the given distribution values on the boundary is termed the geodetic boundary value problem (GBVP). The conventional approach to addressing this boundary value problem involves using spherical harmonic analysis, which successfully represents the external gravitational field through comprehensive coverage of gravitation (or GP) measurements over the Earth's surface or

a surface defined by the orbits of a satellite. Over the past few decades, satellite-based gravity measurement techniques have emerged to surmount challenges related to practical measurements on the Earth's surface, particularly in mountainous and oceanic regions. These techniques have proven instrumental in gravitational field determination.

Kaula [3] introduced a method for formulating a gravity model by calculating the spherical harmonic coefficients based on the observations of orbit perturbations from artificial satellites. This seminal work sparked substantial efforts and led to significant advancements in delineating the Earth's gravitational field using diverse datasets, including satellite radar altimetry data, satellite tracking data, terrestrial gravity data, and combined data sources. The launch of dedicated satellite gravity mapping missions, such as the CHAMP mission in 2000 [4], the GRACE twin satellite mission in 2002 [5], and the GOCE mission in 2009 [6], heightened interest in the recovery of satellite gravitational fields. Furthermore, various techniques have been proposed, including satellite accelerations [7], orbital perturbations [8], harmonic analysis [9], and energy-integral methods [10–12]. These satellite-based gravity measurement approaches are particularly beneficial because they provide comprehensive coverage of the Earth.

Recent advances in time and frequency science have facilitated the development of optical-atomic clocks (OACs), achieving stability and accuracy superior to the 1×10^{-18} level over several hours in laboratory settings [13–15]. Notably, ultra-high-stability onboard and portable satellite clocks are anticipated to become available shortly [16,17]. This development offers the prospect of determining the GP differences between a satellite and a ground station. Precise atomic-clock-related frequency signal links will be utilized, rooted in the principles of general relativity [18]. Consider a scenario in which a satellite transmits frequency signals received by two different ground stations. The GP difference between these stations can be ascertained by observing the frequency shift [19]. However, the precise extraction of the frequency shift attributed to the GP difference between a ground station and a satellite presents challenges. The primary reason is the contamination of observations by the Doppler effect and influences from the ionosphere and troposphere. In response to these difficulties, a more precise formulation of the satellite frequency signal transfer (SFST) approach, based on the tri-frequency combination technique, has been developed [20,21]. This approach aims to determine the GP difference between a satellite and a ground station or between two satellites with an accuracy level of several centimeters when establishing high-precision frequency signal links. For the practical application of the SFST method in geodesy, the relative stability of clocks should reach about 10^{-18} over several hours, corresponding to approximately 1 cm in height.

In the present study, we propose an approach to determine the GP of a LEO satellite along its trajectory, employing the SFST technique. The GP of a LEO satellite can be utilized to construct an Earth Gravitational Model. We refer to the LEO satellite as the Target Satellite (TS) for ease of reference. In Section 2, we provide a concise overview of the SFST technique and the gravitational frequency shift approach, demonstrating how these methods can ascertain the GP difference between a TS and a GEO satellite. Subsequently, we propose an approach to determine a GP distribution over the TS-sphere by establishing frequency links between a TS and three GEO satellites. In Section 3, we conduct simulation experiments under various conditions to evaluate the approach proposed in this study. We summarize the experimental results and discuss potential issues in Sections 4 and 5.

2. Materials and Methods

2.1. Gravity Frequency Shift

General relativity theory proposes a correlation between a clock's frequency and the gravitational potential (GP) at the clock's location. Consider two clocks situated at disparate positions P and Q, with their respective GP values being U_P and U_Q, the frequencies f_P and f_Q of the two clocks conform to a particular equation as delineated in previous studies [22,23].

$$U_P - U_Q = \frac{f_P - f_Q}{f} \cdot c^2 + O(c^{-4}), \tag{1}$$

where c represents the speed of light in a vacuum, and f signifies the average of frequencies f_P and f_Q. Terms on the order of $O(c^{-4})$ denote higher-order terms that may be neglected, specifically when the two stations are near Earth. By accurately measuring and comparing the clock frequencies f_P and f_Q, one can derive the GP difference $U_P - U_Q$ between positions P and Q. Tackling geodetic issues, such as determining GP, using the clock comparison technique is called relativistic geodesy [24,25].

Presently, three methods have been suggested for comparing clocks situated at distinct locations: (1) clock transportation [26,27], (2) transmission of frequency signals via optical fiber links [28–30], and (3) transmission of frequency signals through free-space links and satellites [21,31]. The first two approaches are applicable to terrestrial clock comparisons, while the third is specifically crafted for satellite-based comparisons. However, transferring frequency signals via satellites poses significantly more complexity than what is indicated in Equation (1). For instance, the high-speed motion of the satellite induces Doppler effects. Furthermore, space media, such as the ionosphere and troposphere, can cause frequency shifts during the propagation of microwave or optical signals. To mitigate these issues, Kleppner et al. proposed a technique for transmitting microwave frequency signals between a satellite and a terrestrial site [32]. This method has been successfully applied to validate Einstein's equivalence principle in the Gravity Probe A (GP-A) experiment [33,34].

The crux of the frequency transfer method involves the concurrent connection of a ground site and a satellite through three microwave links, as depicted in Figure 1. A frequency signal f_e is transmitted by ground station E at time t_1, an event denoted as the uplink (represented by a blue line). Upon receipt, satellite S retransmits the received signal f_e' (downlink depicted by the blue line) and emits a new frequency signal f_s at time t_2 (downlink represented by a dark-blue line). These signals are then received at the ground station at time t_3 at position E' as f_e'' and f_s'. Here, ϕ denotes the gravitational potential (GP). In this scenario, most medium influences and the first-order Doppler effect are nullified in the output beat frequency Δf, defined as follows:

$$\frac{\Delta f}{f_e} = \frac{f_s' - f_s}{f_e} - \frac{(f_e'' - f_e') + (f_e' - f_e)}{2f_e}, \tag{2}$$

where f_e and f_s represent frequencies of the signals emitted from the ground site and the satellite. These signals are then received as f_e' and f_s' at the satellite and the ground site, respectively. When the satellite receives the frequency signal f_e', the signal is instantaneously transmitted and subsequently received at the ground site as f_e''. For additional details, please refer to [33].

Kleppner's method was subsequently refined and applied to relativistic geodesy for GP determination [20,21]. This refined method is commonly referred to as the satellite frequency signal transmission (SFST) method. According to SFST, the GP difference between a ground site and a satellite is defined as follows [21]:

$$\frac{\Delta \phi_{es}}{c^2} \equiv \frac{\phi_s - \phi_e}{c^2} = \frac{\Delta f}{f_e} - \frac{v_s^2 - v_e^2}{2c^2} - \sum_{i=1}^{4} q^{(i)} + \Lambda f + O(c^{-5}), \tag{3}$$

where $\Delta\phi_{es}$ is the GP difference between the satellite and the ground station; v_e and v_s are velocities of the ground site and the satellite, respectively. The second term of the Equation's right side contains the second-order Doppler effect. $q^{(i)}$ ($i = 1, 2, 3, 4$) are quantities associated with the velocities and positions of the ground site and satellite, vector potential, second Newtonian potential, and third- and fourth-order terms. Λf shows the correction terms for ionospheric, tropospheric, and tidal effect; $O(c^{-5})$ represents higher-order terms, which can be disregarded due to their negligible impact. For comprehensive details, please refer to [21].
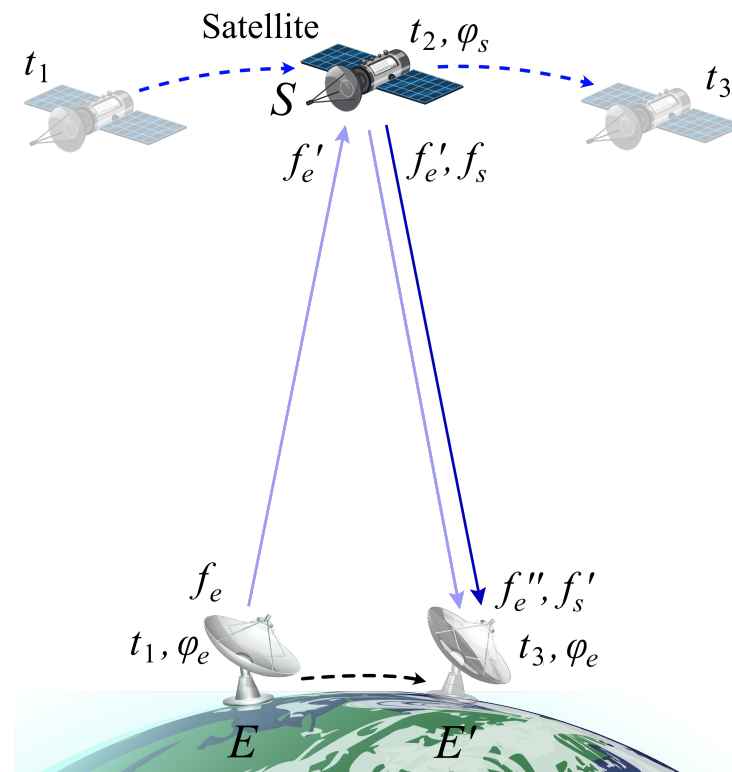
Figure 1. The satellite frequency signal transmission (SFST) technique for determining the gravitational potential difference (GP) between a satellite and a ground site.

The theoretical accuracy of Equation (3) is of the order 10^{-19}, demonstrating a significant improvement over the original formula used in the GP-A experiment, which had an accuracy of approximately 10^{-15}. With the stability of optical-atomic clocks (OACs) achieving a level of 10^{-18}, the SFST technique can yield a measurement of GP with precision to the order of a few centimeters [21].

2.2. Determination of Gravitational Potential along the Target Satellite Orbit

Supposing the GP value of a terrestrial station is known, the GP values for a satellite can be ascertained by establishing SFST links. By determining the GP distribution across a TS sphere (a sphere defined by the orbits of satellites similar to the GOCE or GRACE types), the Earth's external gravitational field can be deduced correspondingly [35]. However, due to the proximity of the satellite's orbit for gravitation measurement (for instance, the altitude of the GRACE satellite is around 500 km), only a short arc length of the orbit is visible to a specific terrestrial station. Ascertaining the GP distribution across the TS sphere would necessitate hundreds of terrestrial datum stations with known GP values to ensure the satellite can continuously connect to at least one terrestrial station at any given time [36]. Furthermore, the majority of Earth's surface is composed of oceans, which further complicates the task of establishing a sufficient number of terrestrial datum stations to meet the observation objectives. Consequently, our capacity to deploy the necessary infrastructure for continuous GP measurement of the target satellite is considerably restricted.

The SFST method described in Section 2.1 was initially conceived for determining the GP difference between a terrestrial station and a satellite. Nevertheless, with some modifications, it can also be adapted to determine the GP difference between two satellites [36]. Imagine a scenario in which a target satellite (TS) in a low Earth orbit is linked to a Geosynchronous Equatorial Orbit (GEO) satellite, herein referred to as GS for simplicity, situated in a higher Earth orbit. The configuration of their inter-satellite SFST links is described as follows.

Referring to Figure 2, a frequency signal f_G is generated by an emitter on the GS at a specific time t_1. This signal is subsequently received by the TS at time t_2. Upon receiving f_G, the TS transmits it back as f'_G and simultaneously emits a new frequency signal f_T. The receiver on the GS, now designated as GS', intercepts both signals (f'_G and f'_T) from the TS at a later time t_3. During the period of signal emission and reception, the GEO satellite's position in space transitions from GS to GS'. The target satellite transmits and emits its signals at the same instant it receives the signal. As such, its position in the signal links is designated as the point TS at time t_2. By setting $f_G = f_T$, the gravitational potential difference between the GS and the TS can be expressed as:

$$\frac{\Delta\phi_{GT}}{c^2} \equiv \frac{\phi_T - \phi_G}{c^2} = \frac{\Delta f}{f_G} - \frac{v_T^2 - v_G^2}{2c^2} - \sum_{i=1}^{4} q^{(i)} + \Lambda f + O(c^{-5}),\tag{4}$$

where the subscripts G and T represent the GS and TS respectively, and the beat frequency Δf is given as:

$$\frac{\Delta f}{f_G} = \frac{f'_T - f_T}{f_G} - \frac{(f''_G - f'_G) + (f'_G - f_G)}{2f_G}.\tag{5}$$

The transmission process might introduce a slight latency, leading to slight discrepancies in the satellite's position between the signal emission and reception times. Considering a signal transponder delay of approximately 800 ns [37] and a typical orbital height of the TS of around 500 km (with a velocity of about 7.6 km/s), the TS moves a mere 0.61 cm between the emission and reception of signals. This minute displacement is negligible for observations requiring a centimeter scale precision level.
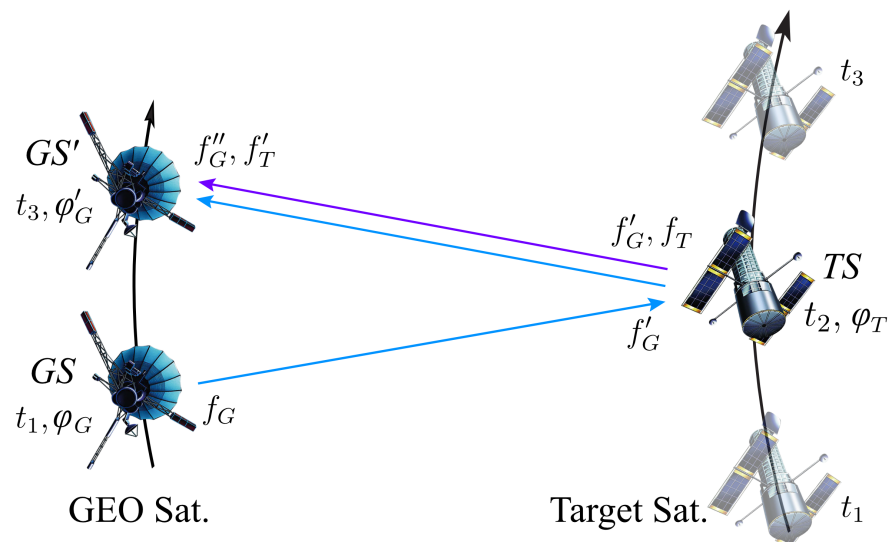
Figure 2. The satellite frequency signal transmission (SFST) technique for determining the gravitational potential difference (GP) between two satellites.

Analogous to the satellite-to-ground link, we postulate that the GP difference between the GS and TS is measured using the SFST method, with the absolute GP values of the GS provided a priori. Consequently, this allows the GP values of the TS to be derived. The altitude of a typical GS is roughly 35790 km above the equator. Referring to Figure 3, in the scenario where the TS is a LEO satellite in a polar orbit, positioned approximately 500 km above the geoid, the distance between the target satellite and Earth's center is about 6870 km. The distance between a GEO satellite and Earth's center is about 42,170 km. When the TS is placed at the poles (N or S), it can connect the GS without being blocked by the Earth. The TS is visible until reaching the P point (if block threshold OH = 6400 km, the angle of PON $\theta = 12.8°$). Thus, only two uniformly distributed GSs are necessary to maintain continuous SFST links between a GS and the TS, enabling the determination of the GP values of the TS's orbital sphere. However, in practical scenarios, it is advisable to employ three uniformly distributed GSs to ensure stable and reliable frequency signal connections (see Section 3.1).
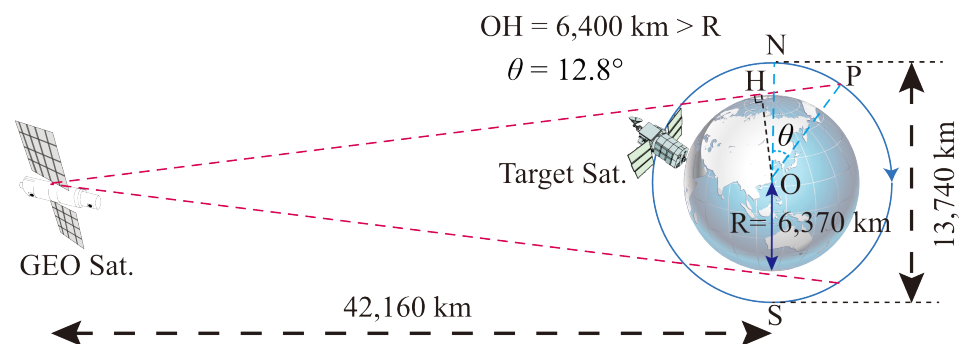

Figure 3. The intervisibility between a GEO satellite and a LEO satellite (the target satellite). The two satellites are intervisible for more than half of the orbit period of the target satellite.

The GP distribution across the TS-sphere allows the gravitational field external to the TS sphere to be derived. Furthermore, employing the spherical harmonic expansion expression, the identified gravitational field can be extended downward to the Earth's surface [38]. Therefore, the GP values over the TS sphere can be used directly to construct an Earth Gravitational Model.

3. Simulation Experiments

In this section, we undertake a series of simulation experiments to substantiate the inter-satellite SFST technique for GP determination over the TS spheres and to establish an Earth Gravitational Model (EGM). Presently, the stability of an onboard satellite atomic clock approximates $10^{-13}\tau^{-1/2}$ (τ in seconds) [17,39]. Nevertheless, the most advanced optical atomic clock currently available on the ground achieves the stability of $9.7 \times 10^{-18}\tau^{-1/2}$ [15]. Therefore, our experiments implement clock stability levels ranging from $10^{-13}\tau^{-1/2}$ to $10^{-17}\tau^{-1/2}$, in anticipation of the eventual integration of superior clocks onboard satellites. We will juxtapose observed GP distributions with their true values at the TS's orbit to assess our approach. Additionally, we will compare the derived EGM and the EGM2008 model [40]. The experiment's framework is depicted in Figure 4. To assess the efficacy of our method, we conduct a comparative study of the observed and true values of the TS's gravitational potential. Additionally, we compare the EGM2008 model with the recovered Earth Gravitational Models up to degree/order 200.
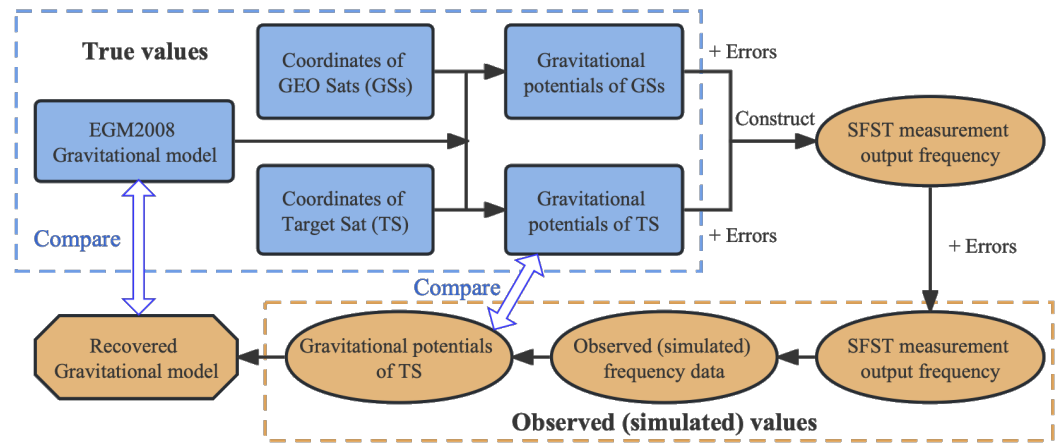
**Figure 4.** The scheme of the simulation experiment.

3.1. Input Data

Section 2.2 demonstrates that a pair of GSs can maintain consistent SFST links to a TS. However, employing three evenly distributed GSs positioned above the equator is preferable for enhanced reliability in real-world applications. For our experiments, we selected the following satellites to serve as GSs: the Chinese communication satellite CHINASAT-1A (at 130.0°E), the European Union meteorological satellite METEOSAT-9 (at 9.2°E), and the US communication satellite ECHOSTAR-10 (at 110.2°W). The GRACE-FO 1 satellite, with an orbit height of approximately 500 km, was chosen as the TS. The configuration for this experiment is illustrated in Figure 5. As the TS orbits the Earth, it maintains SFST links with at least one or two GSs. Leveraging the gravitational potentials known at the GSs, we can effectively determine the gravitational potential at the TS's orbit.
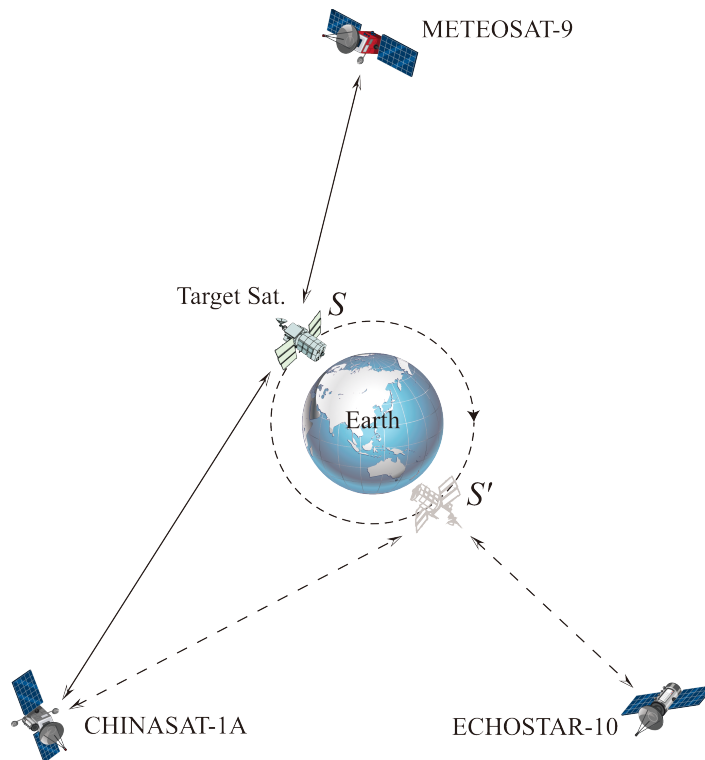
Figure 5. The target satellite (TS) retains consistent connections with three geosynchronous equatorial orbit satellites (GSs).

The orbital period of the TS, specifically GRACE-FO 1, is approximately 1.6 h, with an inclination of about 89°. In order to acquire GP data across its orbital sphere with a resolution of $30' \times 30'$, it is necessary to conduct continuous observations for at least 576 h (or 24.0 days), with the observation interval not exceeding 8.0 s. Consequently, we have established an observational period of 30.0 days with observation interval of 1 s, thereby fully meeting the resolution requirements (see Figure 6). It is pertinent to note that minor unobserved areas exist at the poles due to the TS's inclination not being exactly 90°. However, our computations (detailed in Section 4) indicate that this factor has negligible influence on establishing an EGM. The TS is linked to the closest observable GS for every observation via SFST links. The base frequency, f_G, transmitted by the three GSs is alternately set as 2.8 GHz, 3.0 GHz, and 3.2 GHz. Orbit data for the four satellites (one TS and three GSs) are derived from two-line element (TLE) set data, utilizing the Simplified General Perturbations 4 (SGP4) model [41]. Subsequently, the GPs at the orbits of these satellites can be determined using the EGM2008 model. All these data are treated as true values. Thus, errors associated with orbit data and GP are only considered when we conduct simulated observations.
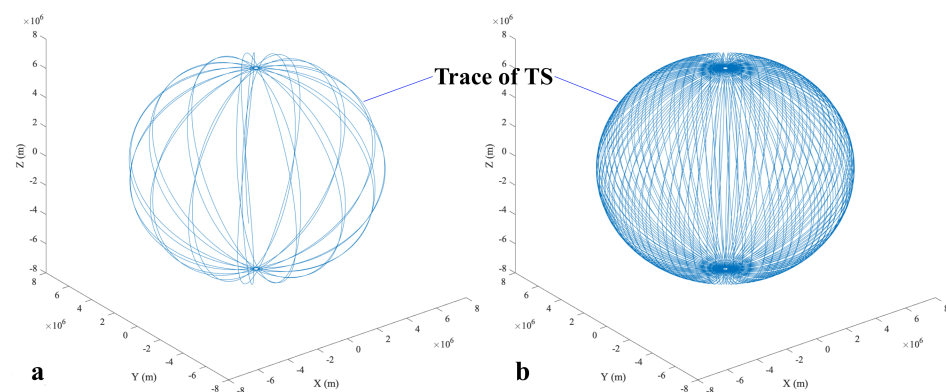
Figure 6. The trace of target satellite (TS) in Earth-centered, Earth-fixed (ECEF) coordinate for (**a**) 1 day and (**b**) 5 days.

The ionospheric and tropospheric conditions significantly impact the frequency of microwave signals. To ascertain the values for electron density, we employed the International Reference Ionosphere (IRI) model [42] as a means to approximate the ionospheric effects [43]. Given the TS's altitude, roughly 500 km, which surpasses the tropospheric layer's extent (typically up to 60 km from the ground), the influence of the troposphere can be considered negligible. The GP at the satellites' orbits is also subject to periodic tidal effects. However, these effects are well modeled [44] and can be effectively mitigated with robust software tools such as Tsoft [45] or ETERNA [46]. Our experiment used a Python library Tidal Potential [47] to construct and analyze tidal signals. The input data are summarized in Table 1.

Table 1. The input data utilized in simulation experiments.

Entities	Values of Parameters
GS Satellite	METEOSAT-9 (f_G = 2.8 GHz)
	CHINASAT-1A (f_G = 3.0 GHz)
	ECHOSTAR-10 (f_G = 3.2 GHz)
TS Satellite	GRACE-FO 1
Gravity field model	EGM2008
Ionospheric model	International Reference Ionosphere
Tide correction	Tidal Potential
Observation duration	1∼30 January 2023
Mearsurement interval	1 s

3.2. The Simulated Observations of GP along the TS Orbit

The next step involves determining the GP values at the TS's orbit once the input data have been established. We consider three GSs, each denoted as GS_i ($i = 1, 2, 3$), respectively. By taking an SFST measurement every 1 s, we can derive an observed GP difference value, $\Delta\hat{\phi}_{GTi}(t)$, according to Equation (4). Assuming the GP of $GS_i(t)$ is provided (denoted as $\phi_{GS_i}(t)$), the observed GP of the TS (denoted as $\hat{\phi}_T(t)$) can be obtained as $\hat{\phi}_T(t) = \phi_{GS_i}(t) - \Delta\hat{\phi}_{GTi}(t)$. Practically, the absolute GP values of the GSs can be calculated using an EGM, such as EGM2008. Given their considerable distance from Earth, the precision of the calculated GPs is relatively high, exceeding 0.1 m^2/s^2. The error in the absolute GP values along the orbits of the GSs is denoted as e_{pot} in Equation (6).

The observed values $\hat{\phi}_T(t)$ differ from the true GP value $\phi_T(t)$ due to the influence of various sources of error. In this simulation experiment, we accounted for clock error (e_{clk}), errors in the satellite's position and velocity (e_{pos} and e_{vel}), ionospheric residual error (e_{ion}), potential errors (e_{pot}), and tidal correction residual error (e_{tide}). The errors above are treated as noises, necessitating their simulation and subsequent addition to the true values based on respective error models. The cumulative errors, e_{all}, are expressed as follows:

$$e_{all} = e_{clk} + e_{ion} + e_{pos} + e_{vel} + e_{pot} + e_{tide}, \tag{6}$$

and the observed values $\hat{\phi}_T(t)$ can be expressed as

$$\frac{\hat{\phi}_T(t)}{c^2} = \frac{\phi_G(t)}{c^2} + \frac{\Delta f(t)}{f_G} - \frac{v_T(t)^2 - v_G(t)^2}{2c^2} - \sum_{i=1}^{4} q^{(i)} + \Lambda f(t) + e_{all}(t). \tag{7}$$

The nature and magnitude of such errors play pivotal roles in this study. Therefore, it is necessary to investigate various error models corresponding to different sources of errors in order to bring the simulation case closer to the real-world scenario.

Initially, we establish the clock error magnitude of e_{clk} as $1.0 \times 10^{-13}\tau^{-1/2}$, which is currently attainable. Given the best contemporary laboratory clocks, which demonstrate stability of $9.7 \times 10^{-18}\tau^{-1/2}$ [15], we reduced the magnitude of e_{clk} to $1.0 \times 10^{-15}\tau^{-1/2}$ and $1.0 \times 10^{-17}\tau^{-1/2}$ to simulate specific cases under varying clock precision levels. Despite numerous types of random noises affecting atomic clock signals [48], white frequency modulation and random walk frequency modulation are the most significant components [49]. Accordingly, the behaviors of clock errors are modeled as follows:

$$e_{clk}(t) = a_{clk} + b_{clk} \cdot t + c_{clk} \cdot w(t) + d_{clk} \cdot \int_0^t \xi(t)\, dt, \tag{8}$$

where a_{clk}, b_{clk}, c_{clk}, and d_{clk} denote constant coefficients, while $w(t)$ and $\xi(t)$ both correspond to standard white Gaussian noises. Each term on the right side of Equation (8) carries a distinct physical implication: a_{clk} signifies the initial frequency difference, $b_{clk} \cdot t$ denotes the drift term, $c_{clk} \cdot w(t)$ represents the white noise component, and $d_{clk} \cdot \int_0^t \xi(t)\, dt$ indicates the random walk effect. A series of frequency comparison data with embedded errors can be generated by assigning suitable values to the constant coefficients based on the performance of OACs, as outlined in [13]. The statistical properties of the three clock error series are illustrated in Figure 7.

The magnitudes of other error sources are substantially smaller when compared to clock errors. These are briefly discussed below, while more detailed explanations can be found in [21].
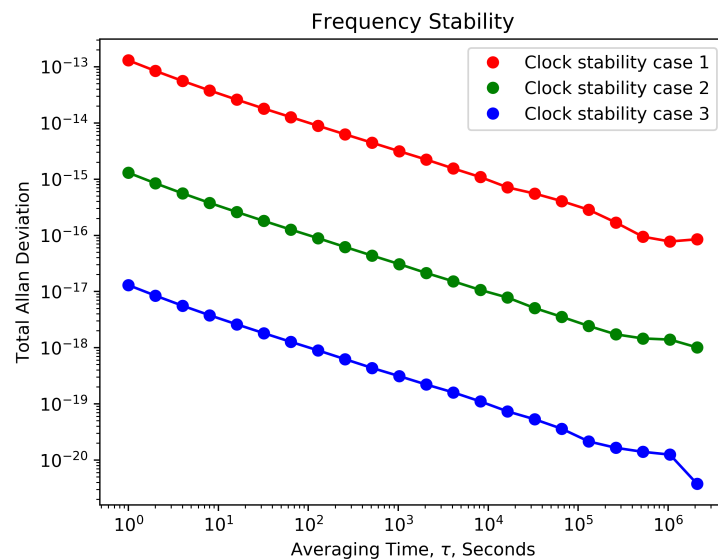
Figure 7. The total Allan deviation for three different clocks. The instabilities of the clocks are $10^{-13}\tau^{-1/2}$, $10^{-15}\tau^{-1/2}$ and $10^{-17}\tau^{-1/2}$ for case 1, case 2 and case 3, respectively.

The impact of satellites' velocity errors is primarily determined by the $(v_T^2 - v_G^2)/(2c^2)$ term in Equation (4). The velocity uncertainty of a spacecraft can reach 0.1 mm/s [50], corresponding to an approximate $e_{vel} \approx 10^{-17}$ in relative frequency. The position errors of satellites influence the determined GP over the TS's orbit since the satellite's GPs are observed at positions divergent from the assumed positions. The magnitudes of these errors can be estimated using the EGM2008 model by determining the GPs of two slightly different positions. The position uncertainty of a GEO or LEO satellite is around 1 dm currently [51,52]. However, it is highly probable that if these satellites are equipped with high-precision atomic clocks, the position uncertainty can be improved to 1 cm. Therefore, in our experiments, we suppose the satellites' position uncertainty is around 1 cm, corresponding to a maximum of 8.5×10^{-2} m^2/s^2 in GP ($e_{pos} < 10^{-18}$ in relative frequency). Similarly, considering the precision of GP values determined by EGM2008 is also about 1 cm in height, the magnitude of potential error e_{pot} is less than 10^{-18} in relative frequency.

The ionosphere's effect on the frequency shift of a one-way signal is presented as [43]:

$$\Delta f_{ion} = -\frac{f}{c}\frac{\mathrm{d}}{\mathrm{d}t}\int_L (n_i - 1)\,\mathrm{d}s, \tag{9}$$

where Δf_{ion} is the frequency shift caused by ionosphere, L shows the path of the signal's propagation, and n_i denotes the phase index of refraction of ionosphere expressed as [53]:

$$n_i = 1 - 40.3\frac{N_e}{f^2} + O(f^{-3}), \tag{10}$$

where N_e represents the electron density per cubic meter and $O(f^{-3})$ designates high-order terms, which are omitted as they are at least two orders of magnitude smaller than the f^{-2} term [54]. The distribution of electron density, N_e, can be acquired from the IRI model, and the path of the frequency signals can be deduced from the satellite orbit data. Therefore, the Δf_{ion} value can be accurately modeled, and only the residual values need to be considered. Furthermore, the electron density is relatively low (the maximum density is at about 350 km height [55]), as the signals between the TS and the GSs are higher than 500 km from Earth's surface. Consequently, in this satellite-to-satellite case, the magnitude of the ionosphere error, e_{ion}, is estimated as 10^{-19} in relative frequency. This magnitude is significantly smaller than the satellite-to-ground case estimated in our previous studies [21].

Tidal effects can be corrected and modeled by the Tidal Potential library. The tidal effects on a satellite are smaller and can be estimated more precisely than on a ground station. We assume that the magnitude of the tidal error, e_{tide}, is approximately 10^{-18} in relative frequency because the tidal effects can be modeled to a precision of several centimeters at a ground station. Table 2 illustrates all errors (or residual errors) magnitudes.

Table 2. Magnitudes of different error sources in determining the gravitational potential difference between the target satellite (TS) and a geosynchronous equatorial orbit satellite (GS). They are transformed to relative frequency.

Influence Factor	(Residual) Error Magnitude in $\Delta f / f_G$
Ionospheric correction residual	$e_{ion} \sim 10^{-19}$
Tidal correction residual	$e_{tide} \sim 10^{-18}$
Position error	$e_{pos} < 10^{-18}$
Velocity error	$e_{vel} \sim 10^{-17}$
Gravitational potential error	$e_{pot} < 10^{-18}$
Clock error	$e_{clk} \sim 10^{-13}, 10^{-15}, 10^{-17}$

Except for clock errors, there are no established mathematical models that simulate the characteristics of other error sources, such as residuals of ionospheric and tidal corrections. Consequently, we implemented a general error model that includes systematic (initial) offset, drift, and white Gaussian noise for each of these error sources, as follows:

$$e_j(t) = a_j + b_j \cdot t + c_j \cdot w_i(t). \quad (j = ion, pos, vel, pot, tide) \tag{11}$$

In this equation, a_j, b_j, and c_j represent constant coefficients that are randomly determined based on the magnitudes of each error source. Although Equation (11) is a simplified model and may not accurately reflect the characteristics of various error sources, it is deemed acceptable because these errors' magnitudes are much smaller than clock errors. Furthermore, the cumulative effect of many varied, minor errors will behave more similarly to white Gaussian noise.

Given Equations (8) and (11), we can generate the noise signals $e_{all}(t)$ term in Equation (7) based on the characteristics and magnitudes of the error sources at any given time. Therefore, we obtain a set of "observed" values, which forms a time series of the TS's GP $\hat{\phi}_T(t)$, as illustrated on the left side of Equation (7). Considering that the TS orbits the entire Earth in approximately 30 days, these values represent the GP at different time points along the TS's orbit. Consequently, we have a set of values $\hat{\phi}_T(x, y, z)$ correlated with orbit data. Upon 30 continuous days (equivalent to 720 h) of observation, a total of 2,592,000 GP points, denoted as $\hat{\phi}_T(x, y, z)$, were distributed over the TS sphere encompassing the Earth.

3.3. Determining the Earth's External Gravitational Field

The GP distribution $\hat{\phi}_T(x, y, z)$ over the TS sphere enables us to estimate the gravitational field outside solid Earth using the least-squares approach. The Earth's GP, V, at an exterior point (r, θ, λ) can be expanded into spherical harmonics [2]:

$$V(r, \theta, \lambda) = \frac{GM}{a} \sum_{n=0}^{N_{max}} \sum_{m=0}^{n} \left(\frac{a}{r}\right)^{n+1} \left(\overline{C}_{nm} \cos m\lambda + \overline{S}_{nm} \sin m\lambda\right) \overline{P}_{nm}(\cos \theta). \tag{12}$$

In Equation (12), r denotes the geocentric radius, while (r, θ, λ) symbolizes a three-dimensional position in the Earth-centered, Earth-fixed (ECEF) reference frame. The variables θ and λ represent spherical co-latitude and longitude, respectively. GM stands for the geocentric gravitational constant, and a is the semi-major axis of the reference ellipsoid. The coefficients $\overline{C}_{nm}$ and $\overline{S}_{nm}$ are the fully normalized GP coefficients describing the Earth's external gravitational field. $\overline{P}_{nm}$ refers to the fully normalized associated

Legendre functions of degree n and order m. Lastly, N_{max} indicates the maximum degree of the harmonic expansion.

In the context of the linear observation as per Equation (12), the statistical and functional models that enable gravitational field recovery from GP distribution observations are established using a standard Gauss–Markov model [56]:

$$\boldsymbol{y} = \boldsymbol{Ax} + \boldsymbol{\epsilon}, \quad E\{\boldsymbol{y}\} = \boldsymbol{Ax}, \quad D\{\boldsymbol{y}\} = \sigma_0^2 \boldsymbol{Q} = \sigma_0^2 \boldsymbol{P}^{-1}, \tag{13}$$

In this formulation, $\boldsymbol{y}$ denotes the vector of GP observations, while $\boldsymbol{A}$ is the design matrix. The vector $\boldsymbol{x}$ symbolizes the GP coefficients $\overline{C}_{nm}, \overline{S}_{nm}$, which are yet to be estimated. The term $\boldsymbol{\epsilon}$ corresponds to the vector of observational errors. $D\{\boldsymbol{y}\}$ represents the error variance–covariance matrix, $\boldsymbol{P}$ is the weight matrix, $\boldsymbol{Q}$ signifies the inverse of the weight matrix, and σ_0^2 is the variance component.

Based on the above-described data processing method, we estimated three recovered Earth Gravitational Models (REGMs) with the degree and order of 200 from GP values distributed over the TS sphere in the three experiment cases. Since the error distribution is unknown in GP observations, we set the weight matrix $\boldsymbol{P}$ as a unit matrix. We consider that the noises in GP observations are white noises. The results are illustrated and discussed in Section 4.

4. Results

We first estimate the precision of the observed GP distributions over the TS sphere. The observed disturbing potentials from three different experimental cases are displayed in Figure 8, with Figure 8a exhibiting the disturbing potential of EGM2008, taken as the reference true values. For case 1, featuring a clock instability of $10^{-13}\tau^{-1/2}$, the outcomes appear to be non-beneficial (refer to Figure 8b). However, a substantial improvement is discerned in the results of case 2 (see Figure 8c) and the outcomes for case 3, which is characterized by a clock instability of $10^{-17}\tau^{-1/2}$, align closely with the true values. The standard deviation (SD) and the mean offset between the true and observed values can be estimated by $\phi_T(t)$ and $\hat{\phi}_T(t)$, which are outlined in Table 3. Specifically, the SDs of GP distribution, equivalent to height over the TS sphere, are 12,815.256 m^2/s^2, 128.086 m^2/s^2, and 1.662 m^2/s^2 for cases 1, 2, and 3, respectively.
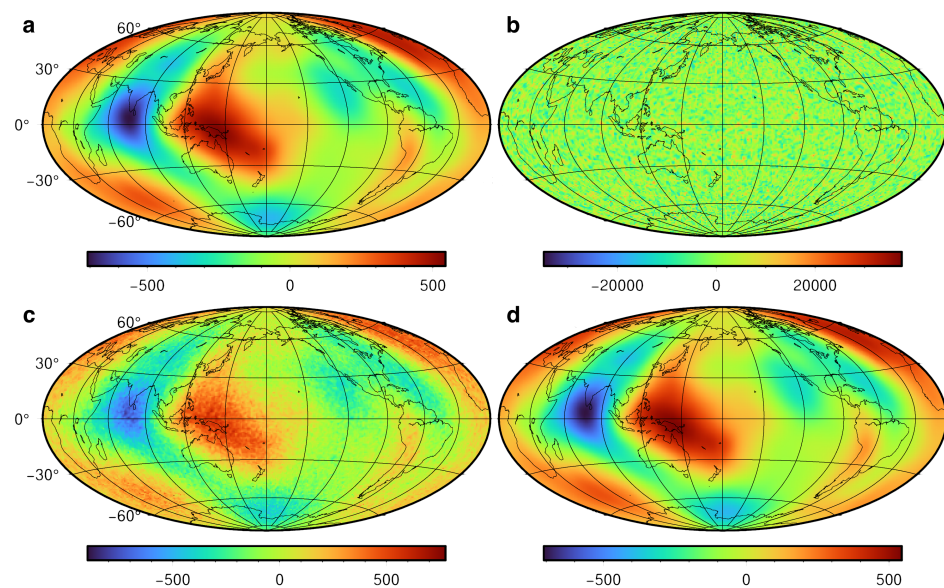
Figure 8. The disturbing potentials (m^{2}s^{-2}) of (**a**) EGM2008 as true values; (**b**) experiment case 1, utilizing clocks with instability of about $10^{-13}\tau^{-1/2}$; (**c**) experiment case 2, using clocks with instability of about $10^{-15}\tau^{-1/2}$; (**d**) experiment case 3, utilizing clocks with instability of about $10^{-17}\tau^{-1/2}$.

Table 3. The statistical information of the GP offset at the target satellite's orbit between true values (calculated by EGM2008) and simulating observations using the SFST method.

Case	Clock Instability	Mean Offset (m²/s²)	Standard Deviation (m²/s²)
1	$10^{-13}\tau^{-1/2}$	1.200	12,815.256
2	$10^{-15}\tau^{-1/2}$	0.243	128.086
3	$10^{-17}\tau^{-1/2}$	-1.86×10^{-3}	1.662

Then, we evaluate the precisions of the REMGs drawing from the GP distributions over the TS sphere. The procedure outlined in Section 3.3 was executed, which led to the procurement of the coefficients for the spherical harmonics expansion formula, as defined by Equation (12). Consequently, the REGMs were formulated. The difference between the coefficients of the REGMs and those of EGM2008 is visually represented in Figure 9.

The outcomes suggest that clock instability greater than $10^{-17}\tau^{-1/2}$, as in cases 1 and 2, leads to diminished precision in the REGMs. However, when the clock instability attains $10^{-17}\tau^{-1/2}$ (case 3), a relatively accurate set of coefficients for orders and degrees lower than 50 can be achieved.

The REGMs' efficacy can also be evaluated by computing the GPs at the TS sphere. The mean offset and SD between the GP distribution over the TS sphere calculated by EGM2008 and REGMs are shown in Table 4. The SDs of the GP distribution over the TS sphere are, respectively, 1320.475 m²/s², 13.231 m²/s², and 0.143 m²/s² for cases 1, 2, and 3.

A comparison of cases 1, 2, and 3 in Table 3 reveals that the SD in Table 4 is approximately one order of magnitude smaller for each corresponding case. This improvement suggests that the GPs calculated by the REGMs demonstrate superior precision compared to directly observed GPs. This can be attributed to the least-squares approach, which operates by smoothing the observations. However, each case has no noticeable improvement in the mean offset.

Table 4. The statistical analysis of the GP offset between the values calculated by EGM2008 (considered as true values) and those calculated by the recovered Earth Gravitational Model (REGMs). The positions cover the target satellite's orbit.

Case	Clock Instability	Mean Offset (m²/s²)	Standard Deviation (m²/s²)
1	$10^{-13}\tau^{-1/2}$	1.063	1320.475
2	$10^{-15}\tau^{-1/2}$	0.243	13.231
3	$10^{-17}\tau^{-1/2}$	-1.08×10^{-3}	0.143
4	$10^{-18}\tau^{-1/2}$	-1.17×10^{-4}	0.014
5	$10^{-19}\tau^{-1/2}$	-2.94×10^{-6}	1.47×10^{-3}
6	0 *	2.74×10^{-8}	6.96×10^{-4}

* This row demonstrates the REGM derived from true GP values; hence, no clock error exists.

In scenarios in which the clock instabilities are improved to the level of $10^{-18}\tau^{-1/2}$ or even $10^{-19}\tau^{-1/2}$, other sources of error, such as velocity error, become the dominant factor in limiting the precision of the recovered coefficients. In these instances, further detailed analysis and corrections are required for various error sources to formulate more effective correction models. As there could be a substantial period for adjusting onboard clocks to the $10^{-18}\tau^{-1/2}$ instability level, we have reserved these investigations for future research. Nonetheless, to underscore the potential of this method, we performed two simplified experiments in which the total error (the summation of clock errors and various other error sources) of SFST links was established at 10^{-18} and 10^{-19}, respectively (as shown in Figure 9d,e).

We observed that by decreasing the total error magnitudes to 10^{-19}, the recovered harmonic expansion coefficients demonstrated commendable quality, closely matching

those recovered from the true values (as indicated in Figure 9f). The REGMs' precision on TS's orbit for cases 4, 5, and 6 are detailed in Table 4.
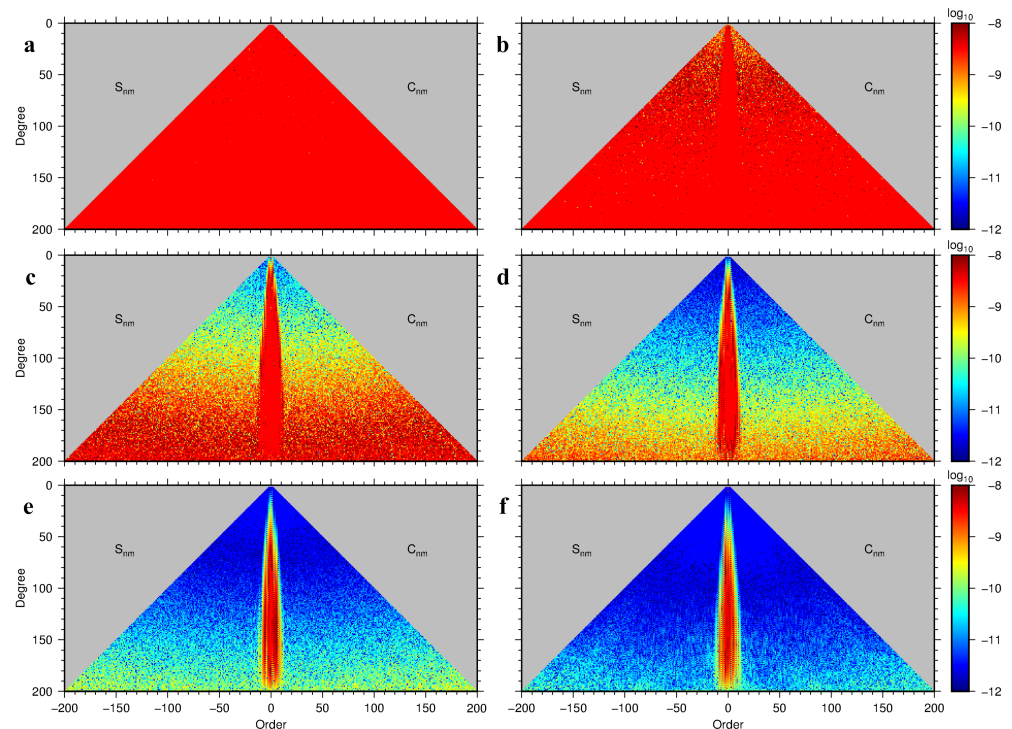
Figure 9. The divergence between the recovered harmonic expansion coefficients and EGM2008. The clock instabilities of various experiments are (**a**) $10^{-13}\tau^{-1/2}$; (**b**) $10^{-15}\tau^{-1/2}$; (**c**) $10^{-17}\tau^{-1/2}$. Figures (**d**,**e**) depict two additional experiments conducted to establish the total error magnitude for an SFST link of 10^{-18} and 10^{-19}, respectively. Figure (**f**) demonstrates the recovered coefficients derived from the true values of GP distribution over the TS-sphere, as defined by EGM2008.

5. Conclusions

In this research, we developed a methodology for calculating the gravitational potentials (GPs) along the orbits of a Low Earth Orbit (LEO) satellite, leveraging precise clocks and inter-satellite frequency signal transfer. We further showcased a potential application of determining the Earth's gravitational field based on the calculated GPs using the satellite frequency signal transfer (SFST) technique.

When the precision of the optical atomic clocks (OACs) is less than $10^{-17}\tau^{-1/2}$, the accuracy of the observed GPs is primarily influenced by the OACs. For example, according to our simulated experiments, the GPs over a target satellite's (TS) orbit can be calculated with precision levels of approximately 12,815.256 m^2/s^2, 128.086 m^2/s^2, and 1.662 m^2/s^2, using clocks with stabilities of $10^{-13}\tau^{-1/2}$, $10^{-15}\tau^{-1/2}$ and $10^{-17}\tau^{-1/2}$, respectively. We can use these GP observations to derive recovered Earth Gravitational Models (REGMs). The precisions of GPs calculated by the REGMs improved approximately one order of magnitude at the TS's position compared to the direct observations, reaching 0.143 m^2/s^2 (equivalent to 1~2 cm) if the clock instability is $10^{-17}\tau^{-1/2}$.

Presently, the stability of a satellite's onboard clock is approximately $10^{-13}\tau^{-1/2}$. However, precise optical atomic clocks have achieved a stability level of $9.7 \times 10^{-18}\tau^{-1/2}$ under laboratory conditions [15]. It is foreseeable that the stability of onboard atomic/optical clocks could attain a similar level in the near future. At this clock stability level, the precision of the GPs ascertained by the inter-satellite SFST method can reach 1.662 m^2/s^2 (see Table 3 case 3, equivalent to 1~2 decimeters), which presents a novel method for obtaining GP data around the Earth, with broad potential applications in geoscience. Suppose the clock stability surpasses $10^{-17}\tau^{-1/2}$, reaching levels such as $10^{-18}\tau^{-1/2}$ or even $10^{-19}\tau^{-1/2}$; then various other sources of error, such as satellite velocity errors and ionospheric correction

residual errors, will become the principal factors affecting the determination of GPs. This instance necessitates the development of more precise error correction models.

Directly applying the GP data around the Earth involves deriving an Earth Gravitational Model (EGM). In this study, we merely demonstrated a rudimentary method for obtaining the REGM without any optimization or fine-tuning. It is advisable to derive an EGM from various data sources and methods in a practical setting. The GP data of a LEO satellite, obtained via the SFST method, is a valuable addition to our current resources, considering we lack a robust method for measuring a satellite's GP.

Author Contributions: Conceptualization, Z.S. and W.S.; methodology, Z.S.; software, Z.S. and X.X.; validation, X.X. and S.Z.; formal analysis, T.Z.; investigation, L.W.; resources, L.H.; data curation, L.H.; writing—original draft preparation, Z.S.; writing—review and editing, Z.C.; visualization, S.X.; supervision, W.S. and S.Z.; project administration, W.S.; funding acquisition, Z.S. and W.S. All authors have read and agreed to the published version of the manuscript.

Data Availability Statement: The data obtained in the study are available from the corresponding author upon reasonable request.

Conflicts of Interest: The authors declare no conflict of interest.

Abbreviations

The following abbreviations are used in this manuscript:

EGM	Earth Gravitational Model.
GEO	Geosynchronous Equatorial Orbit.
GNSS	Global Navigation Satellite Systems.
GOCE	Gravity Field and steady-state Ocean Circulation Explorer.
GP	Gravitational potential.
GRACE	Gravity Recovery and Climate Experiment.
GS	Geosynchronous Equatorial Orbit satellite.
IRI	International Reference Ionosphere.
LEO	Low-Earth Orbit.
OAC	Optical-atomic clock.
REGM	Recovered Earth Gravitational Model.
SD	Standard deviation.
SFST	Satellite frequency signal transfer.
TS	Target satellite.

References

1. Dziewonski, A.M.; Anderson, D.L. Preliminary reference Earth model. *Phys. Earth Planet. Inter.* **1981**, *25*, 297–356. [CrossRef]
2. Hofmann-Wellenhof, B.; Moritz, H. *Physical Geodesy*; Springer: Berlin/Heidelberg, Germany, 2005; pp. 1–405.
3. Kaula, W.M. *Theory of Satellite Geodesy: Applications of Satellites to Geodesy*; Dover Publications: Mineola, NY, USA, 1966.
4. Reigber, C.; Schwintzer, P.; Lühr, H.; Others. The CHAMP geopotential mission. *Boll. Geof. Teor. Appl.* **1999**, *40*, 285–289.
5. Tapley, B.D.; Bettadpur, S.; Watkins, M.; Reigber, C. The gravity recovery and climate experiment: Mission overview and early results. *Geophys. Res. Lett.* **2004**, *31*, L09607. [CrossRef]
6. Drinkwater, M.R.; Haagmans, R.; Muzi, D.; Popescu, A.; Floberghagen, R.; Kern, M.; Fehringer, M. The GOCE gravity mission: ESA's first core Earth explorer. In Proceedings of the 3rd International GOCE User Workshop, Frascati, Italy, 6–8 November 2006; pp. 6–8.
7. Ditmar, P.; van Eck van der Sluijs, A.A. A technique for modeling the Earth's gravity field on the basis of satellite accelerations. *J. Geod.* **2004**, *78*, 12–33. [CrossRef]

8. Hwang, C. Gravity recovery using COSMIC GPS data: Application of orbital perturbation theory. *J. Geod.* **2001**, *75*, 117–136. [CrossRef]

9. Reubelt, T.; Austen, G.; Grafarend, E.W. Harmonic analysis of the Earth's gravitational field by means of semi-continuous ephemerides of a low Earth orbiting GPS-tracked satellite. Case study: CHAMP. *J. Geod.* **2003**, *77*, 257–278. [CrossRef]

10. Jekeli, C. The determination of gravitational potential differences from satellite-to-satellite tracking. *Celest. Mech. Dyn. Astron.* **1999**, *75*, 85–101. [CrossRef]

11. Han, S.C.; Jekeli, C.; Shum, C.K. Efficient gravity field recovery using in situ disturbing potential observables from CHAMP. *Geophys. Res. Lett.* **2002**, *29*, 36-1–36-4. [CrossRef]

12. Visser, P.N.A.M.; Sneeuw, N.; Gerlach, C. Energy integral method for gravity field determination from satellite orbit coordinates. *J. Geod.* **2003**, *77*, 207–216. [CrossRef]

13. Oelker, E.; Hutson, R.B.; Kennedy, C.J.; Sonderhouse, L.; Bothwell, T.; Goban, A.; Kedar, D.; Sanner, C.; Robinson, J.M.; Marti, G.E.; et al. Demonstration of 4.8×10^{-17} stability at 1 s for two independent optical clocks. *Nat. Photonics* **2019**, *13*, 714–719. [CrossRef]

14. Nakamura, T.; Davila-Rodriguez, J.; Leopardi, H.; Sherman, J.A.; Fortier, T.M.; Xie, X.; Campbell, J.C.; McGrew, W.F.; Zhang, X.; Hassan, Y.S.; et al. Coherent optical clock down-conversion for microwave frequencies with 10–18 instability. *Science* **2020**, *368*, 889–892. [CrossRef] [PubMed]

15. Zheng, X.; Dolde, J.; Lochab, V.; Merriman, B.N.; Li, H.; Kolkowitz, S. Differential clock comparisons with a multiplexed optical lattice clock. *Nature* **2022**, *602*, 425–430. [CrossRef] [PubMed]

16. Hannig, S.; Pelzer, L.; Scharnhorst, N.; Kramer, J.; Stepanova, M.; Xu, Z.T.; Spethmann, N.; Leroux, I.D.; Mehlstäubler, T.E.; Schmidt, P.O. Towards a transportable aluminium ion quantum logic optical clock. *Rev. Sci. Instrum.* **2019**, *90*, 053204. [CrossRef]

17. Jaduszliwer, B.; Camparo, J. Past, present and future of atomic clocks for GNSS. *GPS Solut.* **2021**, *25*, 27. [CrossRef]

18. Einstein, A. Die Feldgleichungen der Gravitation. *Sitzungsberichte Königlich Preuss. Akad. Wiss.* **1915**, *25*, 844–847.

19. Shen, W.; Ning, J.; Liu, J.; Li, J.; Chao, D. Determination of the geopotential and orthometric height based on frequency shift equation. *Nat. Sci.* **2011**, *3*, 388–396. [CrossRef]

20. Shen, Z.; Shen, W.B.; Zhang, S. Formulation of geopotential difference determination using optical-atomic clocks onboard satellites and on ground based on Doppler cancellation system. *Geophys. J. Int.* **2016**, *206*, 1162–1168. [CrossRef]

21. Shen, Z.; Shen, W.B.; Zhang, S. Determination of gravitational potential at ground using optical-atomic clocks on board satellites and on ground stations and relevant simulation experiments. *Surv. Geophys.* **2017**, *38*, 757–780. [CrossRef]

22. Weinberg, S. *Gravitation and Cosmology: Principles and Applications of the General Theory of Relativity*; Wiley: New York, NY, USA, 1972.

23. Bjerhammar, A. On a relativistic geodesy. *Bull. Am. Assoc. Hist. Nurs.* **1985**, *59*, 207–220. [CrossRef]

24. Flury, J. Relativistic geodesy. *J. Phys. Conf. Ser.* **2016**, *723*, 012051. [CrossRef]

25. Puetzfeld, D.; Lämmerzahl, C., Eds. *Relativistic Geodesy: Foundations and Applications*; Springer: Cham, Switzerland, 2019.

26. Kopeikin, S.M.; Kanushin, V.F.; Karpik, A.P.; Tolstikov, A.S.; Gienko, E.G.; Goldobin, D.N.; Kosarev, N.S.; Ganagina, I.G.; Mazurova, E.M.; Karaush, A.A.; et al. Chronometric measurement of orthometric height differences by means of atomic clocks. *Gravit. Cosmol.* **2016**, *22*, 234–244. [CrossRef]

27. Grotti, J.; Koller, S.; Vogt, S.; Häfner, S.; Sterr, U.; Lisdat, C.; Denker, H.; Voigt, C.; Timmen, L.; Rolland, A.; et al. Geodesy and metrology with a transportable optical clock. *Nat. Phys.* **2018**, *14*, 437–441. [CrossRef]

28. Takano, T.; Takamoto, M.; Ushijima, I.; Ohmae, N.; Akatsuka, T.; Yamaguchi, A.; Kuroishi, Y.; Munekane, H.; Miyahara, B.; Katori, H. Geopotential measurements with synchronously linked optical lattice clocks. *Nat. Photonics* **2016**, *10*, 662. [CrossRef]

29. Wu, H.; Müller, J.; Lämmerzahl, C. Clock networks for height system unification: A simulation study. *Geophys. J. Int.* **2019**, *216*, 1594–1607. [CrossRef]

30. Shen, Z.; Shen, W.B.; Peng, Z.; Liu, T.; Zhang, S.; Chao, D. Formulation of determining the gravity potential difference Using ultra-high precise clocks via optical fiber frequency transfer technique. *J. Earth Sci.* **2019**, *30*, 422–428. [CrossRef]

31. Deschênes, J.D.; Sinclair, L.C.; Giorgetta, F.R.; Swann, W.C.; Baumann, E.; Bergeron, H.; Cermak, M.; Coddington, I.; Newbury, N.R. Synchronization of distant optical clocks at the femtosecond Level. *Phys. Rev. X* **2016**, *6*, 021016. [CrossRef]

32. Kleppner, D.; Vessot, R.F.C.; Ramsey, N.F. An orbiting clock experiment to determine the gravitational red shift. *Astrophys. Space Sci.* **1970**, *6*, 13–32. [CrossRef]

33. Vessot, R.F.C.; Levine, M.W. A test of the equivalence principle using a space-borne clock. *Gen. Relat. Grav.* **1979**, *10*, 181–204. [CrossRef]

34. Vessot, R.F.C.; Levine, M.W.; Mattison, E.M.; Blomberg, E.L.; Hoffman, T.E.; Nystrom, G.U.; Farrel, B.F.; Decher, R.; Eby, P.B.; Baugher, C.R.; et al. Test of relativistic gravitation with a space-borne hydrogen maser. *Phys. Rev. Lett.* **1980**, *45*, 2081–2084. [CrossRef]

35. Müller, J.; Wu, H. Using quantum optical sensors for determining the Earth's gravity field from space. *J. Geod.* **2020**, *94*, 71. [CrossRef]

36. Shen, Z.; Shen, W.; Zhang, S. Determination of the gravitational potential at GOCE-type satellite orbit using frequency signal transmission approach. In Proceedings of the 20st EGU General Assembly, EGU2018, Vienna, Austria, 8–13 April 2018; p. 19415.

37. Pierno, L.; Varasi, M. Switchable Delays Optical Fibre Transponder with Optical Generation of Doppler Shift. U.S. Patent 8,466,831, 18 June 2013.

38. Heiskanen, W.A.; Moritz, H. Physical geodesy. *Bull. Geod.* **1967**, *86*, 491–492. [CrossRef]
39. Liu, L.; Lü, D.S.; Chen, W.B.; Li, T.; Qu, Q.Z.; Wang, B.; Li, L.; Ren, W.; Dong, Z.R.; Zhao, J.B.; et al. In-orbit operation of an atomic clock based on laser-cooled 87Rb atoms. *Nat. Commun.* **2018**, *9*, 2760. [CrossRef] [PubMed]
40. Pavlis, N.K.; Holmes, S.A.; Kenyon, S.C.; Factor, J.K. The development and evaluation of the Earth Gravitational Model 2008 (EGM2008). *J. Geophys. Res. Solid Earth* **2012**, *117*, B04406. [CrossRef]
41. Croitoru, E.I.; Oancea, G. Satellite tracking using norad two-line element set format. *AFASES* **2016**, *18*, 423–432. [CrossRef]
42. Bilitza, D.; Altadill, D.; Truhlik, V.; Shubin, V.; Galkin, I.; Reinisch, B.; Huang, X. International reference ionosphere 2016: From ionospheric climate to real-time weather predictions. *Space Weather* **2017**, *15*, 418–429. [CrossRef]
43. Namazov, S.A.; Novikov, V.D.; Khmel'nitskii, I.A. Doppler frequency shift during ionospheric propagation of decameter radio waves. *Radiophys. Quantum Electron.* **1975**, *18*, 345–364. [CrossRef]
44. Voigt, C.; Förste, C.; Wziontek, H.; Crossley, D.; Meurers, B.; Pálinkáš, V.; Hinderer, J.; Boy, J.P.; Barriot, J.P.; Sun, H. The Data Base of the International Geodynamics and Earth Tide Service (IGETS). In Proceedings of the 19th EGU General Assembly, EGU2017, Vienna, Austria, 23–28 April 2017; p. 4947.
45. Van Camp, M.; Vauterin, P. Tsoft: Graphical and interactive software for the analysis of time series and Earth tides. *Comput. Geosci.* **2005**, *31*, 631–640. [CrossRef]
46. Wenzel, H.G. The nanogal software: Earth tide data processing package ETERNA 3.30. *Bull. Inf. Marées Terrestres* **1996**, *124*, 9425–9439.
47. Joernc. Tidal-Potential. 2018. Available online: https://github.com/joernc/tidal-potential (accessed on 10 March 2023).
48. Major, F.G. *The Quantum Beat: The Physical Principles of Atomic Clocks*; Springer Science & Business Media: Berlin/Heidelberg, Germany, 2013.
49. Galleani, L.; Sacerdote, L.; Tavella, P.; Zucca, C. A mathematical model for the atomic clock error. *Metrologia* **2003**, *40*, S257. [CrossRef]
50. Sharifi, M.A.; Seif, M.R.; Hadi, M.A. A comparison between numerical differentiation and kalman filtering for a leo satellite velocity determination. *Artif. Satell.* **2013**, *48*, 103–110. [CrossRef]
51. Li, X.; Zhu, Y.; Zheng, K.; Yuan, Y.; Liu, G.; Xiong, Y. Precise Orbit and Clock Products of Galileo, BDS and QZSS from MGEX Since 2018: Comparison and PPP Validation. *Remote Sens.* **2020**, *12*, 1415. [CrossRef]
52. Shen, P.; Cheng, F.; Lu, X.; Xiao, X.; Ge, Y. An Investigation of Precise Orbit and Clock Products for BDS-3 from Different Analysis Centers. *Sensors* **2021**, *21*, 1596. [CrossRef] [PubMed]
53. Davies, K.; Watts, J.M.; Zacharisen, D.H. A study of F 2 -layer effects as observed with a Doppler technique. *J. Geophys. Res.* **1962**, *67*, 601–609. [CrossRef]
54. Hoque, M.M.; Jakowski, N. Higher order ionospheric effects in precise GNSS positioning. *J. Geod.* **2007**, *81*, 259–268. [CrossRef]
55. Rama Rao, P.V.S.; Niranjan, K.; Prasad, D.; Gopi Krishna, S.; Uma, G. On the validity of the ionospheric pierce point (IPP) altitude of 350 km in the Indian equatorial and low-latitude sector. *Ann. Geophys.* **2006**, *24*, 2159–2168. [CrossRef]
56. Harville, D. Extension of the Gauss-Markov theorem to include the estimation of random effects. *Ann. Statist.* **1976**, *4*, 384-395. [CrossRef]